Journal of Catalysis **191,** 384–400 (2000)
doi:10.1006/jcat.1999.2786, available online at http://www.idealibrary.com on IDEAL®

Structure and Catalytic Properties of VO_x/MCM Materials for the Partial Oxidation of Methane to Formaldehyde

H. Berndt,[1] A. Martin, A. Brückner, E. Schreier, D. Müller, H. Kosslick, G.-U. Wolf, and B. Lücke

Institut für Angewandte Chemie Berlin-Adlershof e.V., Richard-Willstätter-Strasse 12, D-12489 Berlin, Germany

Received September 13, 1999; revised December 14, 1999; accepted December 22, 1999

Novel VO_x catalysts have been developed for the partial oxidation of methane to formaldehyde by air. High surface area mesoporous siliceous MCM-41 and MCM-48 materials have been used as supports to disperse vanadium oxide to prevalent monomeric, i.e., isolated vanadium oxide species, being necessary to minimize the consecutive oxidation of the desired product to carbon oxides. On these supports, a higher concentration of isolated active sites can be obtained than on conventional silica supports. Vanadium oxide was deposited by impregnation with aqueous solutions of NH_4VO_3 and $VO(C_2O_4)$, respectively, followed by calcination of the precursor at 873 K for 16 h. The dispersity and the nature of the vanadium oxide species, i.e., their valence state, coordination, and location on and inside the pore walls, were studied by temperature-programmed reduction, potentiometric titration, solid state ^{51}V NMR, ESR, and UV-Vis spectroscopy. FTIR spectroscopy was used to characterize the acidic porperties. Different vanadium oxide species were observed: (i) $V^{IV}O_x$ and $V^{V}O_x$ species anchored to the siliceous MCM walls and (ii) $V^{IV}O_x$ and $V^{V}O_x$ species incorporated into the pore walls. $V^{V}O_x$ species anchored to the surface showed properties similar to those on conventional VO_x/SiO_2 catalysts. However, it was found that the VO_x species carry acidic V–OH groups, at least partially. The catalytic properties of the catalysts were tested in a plug flow reactor. Reaction orders with respect to methane and oxygen, respectively, as well as the apparent activation energy were comparable with those reported for vanadium oxide supported on precipitated silica, pointing to similar active sites. However, significant higher space-time yields of formaldehyde could be achieved amounting to about 2.2 $kg \cdot kg_{cat}^{-1} \cdot h^{-1}$. Increased activity during cofeeding of steam could be observed due to the generation of $V^{V}O(OH)_x(OSi{\equiv})_{3-x}$ surface species or the corresponding "reduced sites" $V^{IV}O(OH)_x(OSi{\equiv})_{2-x}$ supposed as genuine active sites.

Key Words: **vanadium oxide catalysts; mesoporous supports; siliceous MCM-41 and MCM-48; TPR; ESR; ^{51}V NMR; UV-Vis, FTIR spectroscopy; methane oxidation; formaldehyde production.**

INTRODUCTION

Formaldehyde is an important base product of the chemical industry conventionally produced by catalytic oxidation or oxidative dehydrogenation of methanol. The latter is mainly produced from methane by steam reforming followed by conversion of synthesis gas to methanol. Intensive efforts have been made for a long time to develop a heterogeneous catalytic process for direct synthesis of formaldehyde by partial oxidation of methane. Reports on various suitable catalytic systems have been presented and reviewed in many papers, e.g., (1–9). Several catalyst systems have been studied for this reaction, e.g., promoted zeolites (10, 11), various mixed oxides such as FeNbB oxide (12), Bi_2O_3/SnO_2 (13), or Fe_2O_3/MoO_3 (14), and supported transition metal oxides, particularly silica-supported molybdenum oxide (4, 9, 15, 16) or vanadium oxide (4–9, 17), and, recently, $FePO_4$ on silica (18). The superior performance of silica-supported transition metal oxide catalysts in the heterogeneous partial oxidation of methane to formaldehyde is generally recognised (3).

However, independent of the kind of the catalysts, formaldehyde is obtained in low yields only (below 4%) upon single pass in this process up to now. On the one hand, the formaldehyde formation is thermodynamically favourable at high temperatures (above 873 K), being necessary to activate the relative inert methane on MoO_x/SiO_2 and VO_x/SiO_2 catalysts. On the other hand, the oxidation of methane to carbon oxides is more favoured than the partial oxidation because the activation of a C–H bond in the desired product is easier than the one in the reactant (19). Consequently, there is an interdependence of conversion and selectivity, resulting in an insufficient formaldehyde yield.

Currently, different strategies are pursued to overcome the large difference of reactant-product reactivity/stability and to improve the process for an industrial application:

(i) Enhancement of the yield by means of reaction engineering such as quenching of the formaldehyde in water films on cooled outer reactor walls or inner condenser

[1] To whom correspondence should be addressed. Fax: +49-30 6392 4350. E-mail: h.berndt@aca-berlin.de.

0021-9517/00 $35.00

areas located in the reaction zone of wall reactors (20, 21) or operation in continuous flow recycle mode with product separation (22);

(ii) Search for more selective catalysts in order to improve the yield, e.g., supported iron phosphate (18); and

(iii) Development of improved catalyst systems for enhancement of the space-time yield (STY), e.g., by use of cocatalysts for methane activation (3, 23).

Up to now, the highest STY could be obtained with vanadium oxide highly dispersed on precipitated silica. Generally, isolated or low-oligomeric VO_x species are suggested as sites for the partial oxidation of methane. "Reduced sites," "reduced sites in concerted action with gas-phase oxygen" (24, 25), and "short-lived oxygen species" adsorbed on vanadium oxide sites (26), respectively, have been proposed as genuine active sites.

Site isolation is necessary to control the consecutive oxidation. So, the loading of conventional silica materials (e.g., Cab-O-Sil) with monomeric or mononuclear VO_x species is limited to <5 wt% V_2O_5, because at higher loading "bulk-like" V_2O_5 is preferentially formed (8).

Kinetic studies have shown that formaldehyde is the primary product whereas CO and CO_2 are mainly formed in consecutive reactions (27–30). Consequently, very short modified residence times are used in this process: However, a slow diffusion of the formaldehyde out of the pore system of the catalysts may still favour consecutive total oxidation.

In several papers an improvement of the formaldehyde yield by steam cofed to the educt stream has been reported. Herman *et al.* demonstrated a drastic increase of the STY of formaldehyde and an additional formation of methanol (3). Whereas the increased methanol formation could be related to a favoured hydrolysis of surface methoxy species, no explanation was given for the enhanced formaldehyde formation. In the case of MoO_3/SiO_2 catalysts it was concluded that silicomolybdic acid is reversibly formed from highly dispersed MoO_3 and the consecutive oxidation of formaldehyde is depressed (31). A selectivity increase was also observed on $FePO_4/SiO_2$ catalysts (18). It was suggested that P–OH groups formed by reversible cleavage of P–O–P bonds influence the catalytic properties of the active iron species.

The aim of our study was to develop VO_x catalysts with a higher concentration of isolated VO_x species and favourable conditions for mass transfer in order to enhance the STY of formaldehyde. Therefore, we studied the potential of the mesoporous siliceous materials MCM-41 and MCM-48 as supports for highly dispersed vanadium oxide species. These materials originally developed by Mobil Oil and designated as M41S (32) stand for thermally stable high surface areas (>500 m^2/g) and tubular pore systems with relatively large pore diameters of 2–3 nm. Monomeric or low-oligomeric vanadium oxide species can be anchored to silanol groups of these new silica materials in a similar way as on conventional silica gel supports as has been demonstrated by Grubert *et al.* (33) and Morey *et al.* (34), respectively. The present paper describes the preparation of VO_x/MCM-41 catalysts, the characterization of their VO_x species by temperature-programmed reduction (TPR), ^{51}V NMR, UV-Vis, ESR, and FTIR spectroscopy as well as their catalytic performance. The nature of the VO_x species of the VO_x/MCM-41 catalysts is compared with that of conventional VO_x/SiO_2 catalysts described in the literature. Furthermore, the role of steam cofed into the methane-air educt stream is investigated.

EXPERIMENTAL

Catalysts

Catalysts with vanadium oxide loadings of 2, 5, and 10% V_2O_5 (0.5, 1.1, 2.8, and 5.5 wt% V) were prepared by impregnation of conventionally synthesized siliceous MCM-41 or MCM-48 materials (35, 36). The surface area of the parent MCM-41 amounted to 810 m^2/g and MCM-48 to 905 m^2/g. Of the support material 15 g was added to 100 ml of aqueous solution of the corresponding amounts of NH_4VO_3 or $VO(C_2O_4) \cdot 5H_2O$ in a 500-ml vessel of a vacuum rotary evaporator. The slurry was evacuated for a short time to remove air from the pores, and then the vessel was rotated for 1 h, and finally, the water was slowly evaporated at 323 K. The solid product was dried at 393 K for 8 h and finally calcined at 873 K in air for 16 h. The catalyst powder was pressed and afterward crushed, and a sieve fraction of 0.4 to 1.25 mm was used for catalytic testing.

The theoretical vanadium content corresponding to the amount of the precursor used is included in the sample designation (Table 1). The real vanadium content was determined by potentiometric titration after dissolution in H_2SO_4 (see below) and by inductively coupled plasma-optical emission spectrometry (ICP-OES) after

TABLE 1

Survey on the Samples of the VO_x/MCM Catalysts, the Used Precursor, and the Composition

Sample	Vanadium precursor	Vanadium content potentiometric titration (wt%)	Vanadium content ICP-OES (wt%)
0.5V/MCM-41	NH_4VO_3	0.55	—
1.1V/MCM-41	NH_4VO_3	1.12	1.09
2.8V/MCM-41	NH_4VO_3	2.59	2.44
2.8V/MCM-41*	$VO(C_2O_4)$	2.50	—
5.5V/MCM-41	NH_4VO_3	—	4.60
2.8V/MCM-48	NH_4VO_3	2.32	2.82

microwave-assisted dissolution of the samples in HF/HNO_3 up to 8 bar, respectively.

Characterization

Nitrogen physisorption. Nitrogen adsorption/desorption at 77 K were measured using Gemini III equipment (Micromeritics). The specific surface area was calculated following the method of Brunauer, Emmet, and Teller (BET). The method of Barret, Joyner, and Halenda (BJH) was used to determine the pore size distribution (37).

Potentiometric titration of the average vanadium valence state. The supported vanadium oxide was treated with 18 N H_2SO_4 under nitrogen atmosphere. The obtained slurry, containing the dissolved vanadium and the undissolved support, was diluted to an 8 N H_2SO_4 solution. The content of V^{III}, V^{IV}, and V^{V} species was determined using a potentiometric titration method originally introduced by Niwa and Murakami (38). N/100 $(NH_4)_2Fe(SO_4)_2$ standard solution was used for reduction of V^{V} to V^{IV} and N/100 $Ce(SO_4)_2$ for oxidation of V^{III} and V^{IV} to V^{V}, respectively.

Temperature-programmed reduction (TPR). The reduction behaviour of the vanadium oxide species deposited on the tube walls of the MCM-41 was studied by means of TPR (AMI-1 equipment, Altamira/Zeton) using the following parameters: Sample weights of 0.1 g, flow of 5% H_2-Ar with a rate of 50 ml/min, heating rate of 10 K/min, isothermal hold at a final temperature of 1173 K for 0.5 h. Water formed or desorbed during the TPR was removed by molecular sieve 4A before the flow passes the thermal conductivity detector (TCD). The peak area of the hydrogen consumption plot was calibrated by argon pulses into the TPR gas flow.

^{51}V NMR investigations. The structure of $V^{V}O_x$ species anchored on the support surface was investigated by ^{51}V NMR measurements carried out with samples prepared and stored under air or dehydrated and hydrothermally treated, respectively. Solid-state NMR spectra were recorded at 7.0 T on a Varian Unity Plus-300 spectrometer. Static and MAS ^{51}V NMR spectra were measured at 78.9 MHz using a Doty supersonic probe (zirconia rotors 5 mm in diameter). Short excitation pulses of 1 μs duration and recycle delays of 1 s were applied. The maximum spectral width was limited to 100 kHz due to a slow digitizer. Employing only single one-pulse techniques, the resulting spectra are distorted by receiver dead-time effects. As outlined below in detail the apparent peaks of the distorted spectra correspond with the slopes and singularities of the undistored lineshape reported in Ref. (39). The chemical shifts are given in ppm related to $VOCl_3$.

To study the structure of the $V^{V}O_x$ sites in the dehydrated state a sample was heated in the rotor up to 723 K, subsequently cooled down in a desiccator, and sealed.

ESR spectrometric investigations. ESR spectra of $V^{IV}O_x$ species were measured using the c.w. spectrometer ELEXSYS 500-10/12 (Bruker) in X band. Spectra at 77 K were recorded using a finger dewar whereas those at lower temperature were obtained with a helium cryostat and a variable temperature control unit (Bruker). The magnetic field was measured with respect to the standard 2,2-diphenyl-1-picrylhydrazyl hydrate (DPPH). For spectra simulation the computer program of Lozos *et al.* was used (40). Calculations were based on the spin-Hamiltonian

$$H = \beta \cdot S \cdot \mathbf{g} \cdot B + S \cdot \mathbf{A} \cdot I,$$

where β is the Bohr magneton, S is the electron spin operator, $\mathbf{g}$ is the g tensor, B is the magnetic field vector, $\mathbf{A}$ is the hyperfine tensor, and I is the nuclear spin operator.

UV-Vis spectroscopic investigations. In situ UV/VIS-DRS measurements were performed using a Cary 400 UV/VIS spectrometer (Varian) equipped with an *in situ* diffuse reflectance accessory (praying mantis, Harrick) in order to characterize the coordination of the vanadium in monomeric VO_x species, the presence of oligomeric VO_x species, and changes of the vanadium valence state upon reductive and oxidative sample treatment, respectively. V/MCM samples were used as powders diluted with the parent vanadium-free MCM-41 in a ratio of 1 : 10 to reduce light absorption. The reflectance spectra were converted into the Kubelka-Munk function $F(R)$ which is proportional to the absorption coefficient for sufficiently low $F(R)$ values (41). Spectra were deconvoluted into Gaussian bands using the GRAMS/386 program (Galactic Industries Corporation).

FTIR spectrometric investigations. In order to characterize the acidity of the catalysts, spectra in the OH vibration region as well as spectra of chemisorbed pyridine were monitored on a IFS 66 spectrometer (Bruker) using self-supporting wafers in a heatable IR gas cell. The samples were pretreated at 723 K for 1 h under vacuum prior to pyridine adsorption. Pyridine was adsorbed at room temperature from an argon flow containing 2 vol% pyridine. Then, the samples were heated to 373 K and evacuated to remove physisorbed and weakly chemisorbed pyridine. Temperature-programmed desorption of the adsorbed pyridine starting at 373 K was studied by stepwise heating of the sample under vacuum to characterize the strength of the acid sites. Difference spectra were obtained by subtracting the background (base spectrum) of the unloaded sample.

To study possible structural changes by interaction of water vapour with the catalyst surface, a self-supporting wafer prepared from 2.8V/MCM-41 was *ex situ* hydrothermally treated at 873 K for 0.5 h in an argon flow containing 12 vol% water vapour. Afterward the wafer was cooled under the wet flow to 373 K. Then the wet flow was replaced

by a dry argon flow and the sample was cooled to room temperature. After transfer of the sample into the IR cell it was evacuated at 373 K for 10 min. After the background spectrum was recorded, pyridine adsorption was studied again.

Catalytic testing. The catalytic properties of the samples were investigated in a plug flow reactor using a reactor system RIG 100 (ISRI) equipped with several gas flow lines with mass flow controllers to supply the educt stream containing CH_4, air, and nitrogen. Water vapour was fed using a metering pump and an evaporator. The diameter of the quartz tube reactor was 12 mm in the range of the catalyst layer and narrowed down to 6 mm afterward to increase the flow rate and in this way to avoid consecutive reactions of the formaldehyde in the gas phase. Samples (50 and 100 mg) of the catalyst (sieve fraction of 0.4 to 1.25 mm) were mixed with an equal amount of quartz grains of the same size for a better temperature control of the strongly exothermic reaction. In this paper, gaseous hourly space velocity (GHSV) and STY are related to the catalyst weight. The product flow was stripped from formaldehyde and methanol by a water-filled trap at 273 K. The amounts of both products accumulated during a reaction period of 1 h at steady-state conditions were analyzed by means of GC using a DB-WAX capillary column (30 m $\times$ 0.53 mm, 0.5 μm) and a thermal conductivity detector (TCD). The concentration of formaldehyde was additionally checked by iodometric titration (42). Formation of low amounts of gaseous hydrocarbons was observed by GC using a GS-Q column (30 m $\times$ 0.32 mm) and a flame ionisation detector (FID). CO and CO_2 formed were continuously determined by nondispersive IR photometry. Methane conversion was not determined but calculated from the products analyzed. In kinetic studies the partial pressures of methane and oxygen were varied at constant GHSV by addition of nitrogen to the methane-air flow. In catalytic testing with cofeeding of steam the GHSV was held constant by corresponding substitution of nitrogen added to the methane-air stream previously.

RESULTS

Catalysts Characterization

Results of Physisorption Measurements

The specific surface area (S_{BET}) of the freshly prepared catalysts is lower than that of the unloaded supports and decreases with increasing VO_x loading (Table 2). After catalytic testing S_{BET} is further lowered but it remains significantly higher than the specific surface area of V_2O_5/SiO_2 catalysts prepared by use of "pyrolytic" silica Cab-O-Sil M5 or 250 MP (Grace) and "precipitated" silica D11-11 (BASF) or PS (Si 4-5P Grade, Akzo) (8, 24) ($S_{BET} < 250$ m^2/g). Values of the specific surface area of V_2O_5/SiO_2 catalysts used were not reported in these references.

TABLE 2

Specific Surface Areas of the VO_x/MCM Catalyst and the Parent Supports

Sample	S_{BET} ($m^2 \cdot g^{-1}$)
MCM-41	810
1.1V/MCM-41	684
2.8V/MCM-41	676
2.8V/MCM-41*	682
5.5V/MCM-41	656
2.8V/MCM-41 (used)	447
MCM-48	950
2.8V/MCM-48	878

*Precursor $VO(C_2O_4)$.

The pore size distribution of the sample 2.8V/MCM-41 (Fig. 1) shows that the mesoporous structure of the support has been preserved. However, the cumulative pore volume decreased from 0.82 to 0.58 cm^3/g. A similar decrease of the S_{BET} has been already reported by Morey *et al.* for VO_x/MCM-48 samples and was related to a "contraction of the mesoporous tubes" by anchoring of the VO_x species on the tube walls which was derived from XRD data (34).

Results of Potentiometric Titration

Cerimetric titration unambiguously revealed that catalysts freshly calcined as well as catalysts used contain a remarkable part of vanadium in a valence state lower than five (Table 3). However, it is not possible to distinguish

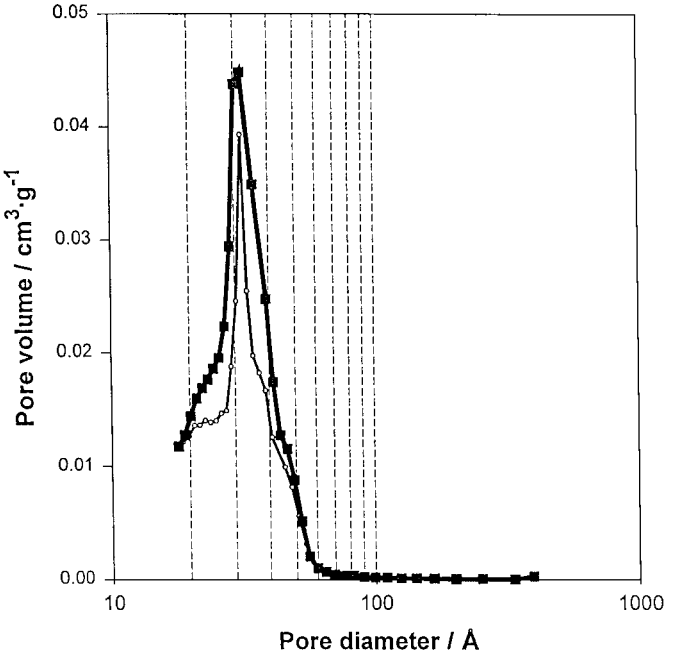

FIG. 1. Pore size distribution of the catalyst sample 2.8V/MCM-41 (thin line) and of the parent siliceous MCM-41 (thick line).

TABLE 3

Results of Temperature-Programmed Reduction and Potentiometric Titration

Sample	V ($mmol \cdot g^{-1}$)	Hydrogen consumption ($mmol \cdot g^{-1}$)	Average valence state of vanadium (TPR)	Average valence state of vanadium (pot. titr.)
0.5V/MCM-41	0.11	0.063	4.17	4.3
1.1V/MCM-41	0.22	0.126	4.15	4.5
2.8V/MCM-41	0.51	0.423	4.66	4.7
2.8V/MCM-41*	0.49	0.405	4.65	4.8
5.5V/MCM-41	0.90	0.808	4.80	4.4
2.8V/MCM-48	0.55	0.483	4.76	4.8
2.8V/MCM-41 (used)	0.53	0.420	4.58	4.2
5.5V/MCM-41 (used)	0.88	0.821	4.88	4.6
2.8V/MCM-41 (treated in H_2O/O_2)	0.50	0.457	4.83	4.7

*Precursor $VO(C_2O_4)$.

between V^{III} and V^{IV} species because a synproportionation of V^{III} and V^{V} ions upon dissolution of the VO_x species cannot be excluded. The average valence state of the vanadium was calculated from the results of the titration with Ce^{IV} and Fe^{II} standard solutions as mentioned above and is compared in Table 3 with the corresponding values determined by TPR. In the case of catalysts with high vanadium loading the total vanadium content determined by titration was a little lower than the one determined by ICP-OES. Obviously, H_2SO_4 is not able to remove all vanadium oxide species from the support in contrast to the complete dissolution of the catalysts by HF/HNO_3 for ICP-OES analysis. Therefore, the results of ICP-OES analysis were used to calculate the average vanadium valence state from TPR results.

TPR Results

The profiles of all the catalyst samples (Fig. 2) show a peak with a maximum around 800 K and a shoulder at its high temperature flank. In agreement with TPR investigations of VO_x/SiO_2 catalysts of Koranne *et al.* (6) and Arena *et al.* (43) the peak can be attributed to the reduction of monomeric or low-oligomeric VO_x surface species. The shoulder reveals a portion of "bulk-like" V_2O_5. At increasing vanadium loading of the V/MCM-41 catalysts the share of the area of the shoulder in the total peak area is approximately constant and furthermore, it is essentially lower than in plots of VO_x/SiO_2 catalysts of comparable vanadium loading (8). In case of the sample 2.8V/MCM-48 a smaller peak and a larger shoulder were obtained compared to the plot of the sample 2.8V/MCM-41. TPR plots of used samples show a slightly larger shoulder referring to increasing portions of bulk-like V_2O_5 (Fig. 3). However, the main portion of the vanadium oxide is still highly dispersed. Similar plots were obtained for 2.8V/MCM-41 samples treated in an oxygen flow, containing 18 vol% water vapour at temperatures of the catalytic testing (873 K) for 0.5 h. This treatment was performed in context with the investigation of an activity improvement observed by cofeeding of steam in the catalytic testing (see below).

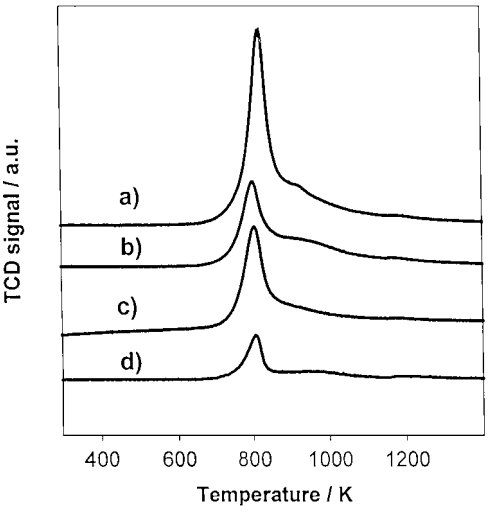

FIG. 2. TPR plots of V/MCM catalyst samples: (a) 5.5V/MCM-41, (b) 2.8V/MCM-48, (c) 2.8V/MCM-41, and (d) 1.1V/MCM-41.

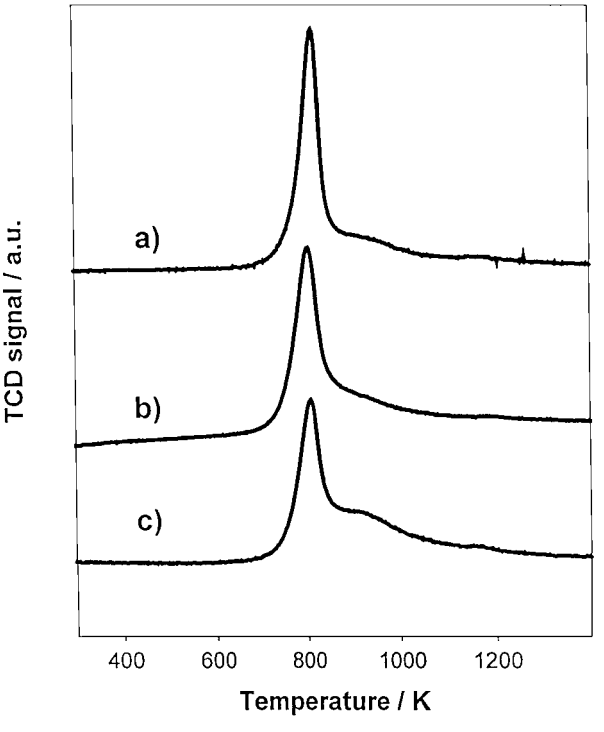

FIG. 3. TPR plots of the sample 2.8V/MCM-41: (a) freshly prepared, (b) used in catalytic testing, and (c) hydrothermally treated.

The hydrogen consumption calculated from the total peak area (Table 3) was significantly lower than the one necessary for a complete reduction of V^V to V^{III} and does not depend on the valence state of the vanadium in the precursor used for impregnation of the MCM-41 support. In principle, the deficit of the hydrogen consumption could have several reasons, namely an incomplete reduction of V^V species to V^{III} species (i.e., partial reduction to V^{IV}), a presence of a portion of V^{IV} or V^{III} species, and/or a presence of nonreducible V^V species in the V/MCM-41 samples. An incomplete reduction of V^V to V^{III} species was reported by several authors for VO_x/SiO_2 catalysts (8, 43, 44); nonreducible V^V and V^{IV} species were observed in V/MCM-41 samples, e.g., by Grubert *et al.* (33) and by Luan *et al.* (45), respectively.

The average vanadium valence state given in Table 3 was calculated assuming a complete reduction of the reducible V^V species to V^{III} species. In most cases, these values are in close agreement with those determined by potentiometric titration. This suggests that in the original catalyst a part of V^{IV} or V^{III} species is present, which is stabilized against oxidation to V^V upon calcination in air. Oxidative treatment in the presence of water vapour results in an increase of the average valence state of the vanadium as determined by TPR. However, no significant change was observed for the same sample by means of potentiometric titration. This points to the idea that oxidized species are located inside the pore walls, which are not soluble by the applied H_2SO_4 treatment.

^{51}V NMR Results

Solid-state ^{51}V NMR spectra were measured to elucidate the location of the oxidic V^V species on the pore walls and/or inside the pore walls. In this study the central transition of the quadrupolar ^{51}V nucleus ($I = 7/2$) was detected which is dominated by strong chemical shift interaction at the field strength of 7.0 T applied. In Fig. 4 the static ^{51}V NMR spectra of the MCM-41 samples loaded with different amounts of vanadium oxide are shown. The broad lineshapes recorded with conventional one-pulse techniques are distorted due to receiver dead-time effects. Das *et al.* (39) presented undistorted lineshapes obtained by using spin-echo pulse techniques. Our spin-echo pulse experiments on reference compounds such as NH_4VO_3 and V_2O_5 on a Varian Unity Plus-500 spectrometer with a fast digitizer confirmed their results. Comparison of these spectra with those obtained by simple one-pulse techniques showed that the apparent peaks of the distorted spectra correspond with the slopes and singularities of the undistorted lineshape. As reported in earlier studies (8, 34, 46, 47) sample treatments such as calcination and rehydration cause shifts of the low-field component $\delta_\perp$ of the tensor of the chemical-shift anisotropy. Such influences are accordingly reflected in the position of the apparent peaks of our distorted spectra, too.

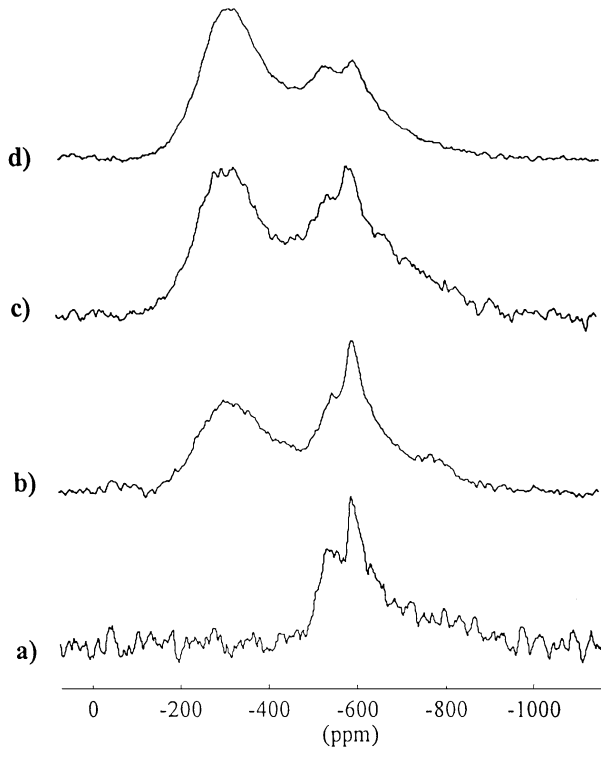

FIG. 4. ^{51}V NMR solid-state spectra of V/MCM-41 catalysts containing different amounts of vanadium: (a) 0.5V/MCM-41, (b) 1.1V/MCM-41, (c) 2.8/MCM-41, (d) 5.5V/MCM-41; all the samples stored under ambient conditions.

The observed spectral features reflect the environment of the ^{51}V sites such as symmetry and coordination to oxygen. For low vanadium content (0.5 wt%) a structured signal with peaks at -536 and -590 ppm dominates. With increasing amounts of vanadium an additional peak at -300 ppm arises. These apparent peaks correspond with the low-field component $\delta_\perp$ of the chemical-shift anisotropy tensor with nearly axial symmetry. The arising peak at -300 ppm is assigned to distorted octahedral (pseudo-octahedral) vanadium species at the surface, whereas the apparent peaks at -536 and -590 ppm have been attributed to vanadium in pseudo-tetrahedral symmetry (34, 48). After dehydration of the surface the low-field peak at -300 ppm disappears and can be reversibly restored under the influence of water vapour under ambient conditions (Fig. 5). These results suggest that the pseudo-tetrahedral $V{=}O(OSi{\equiv})_3$ species at the surface are converted to pseudo-octahedral $V{=}O(H_2O)_2(OSi{\equiv})_3$ species by coordination of water molecules as previously concluded for V^VO_x species on silica (8, 39, 46) and MCM-48 (34), respectively. However, the part of V^VO_x species consisting of the peak at -536 and -590 ppm is very likely inaccessible or unable to coordinate water molecules because these species are probably incorporated into the amorphous pore walls. This kind of species predominates in the sample with the

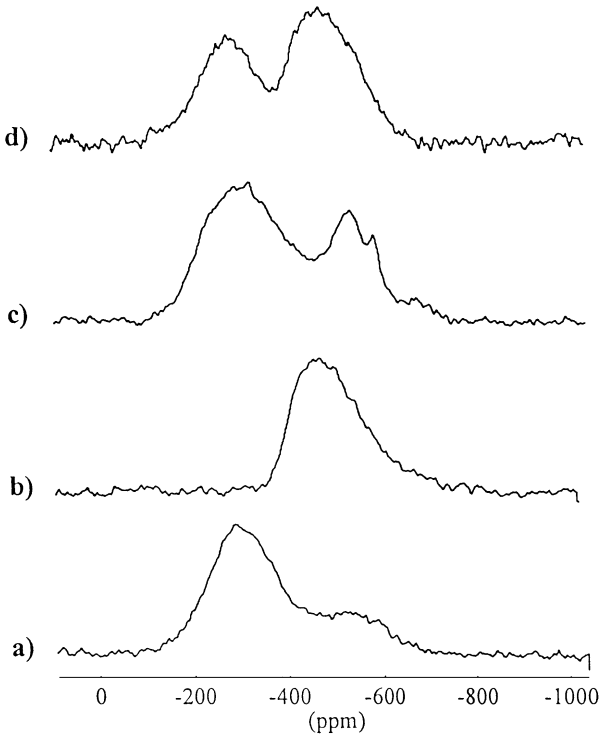

FIG. 5. ^{51}V NMR solid-state spectra of the sample 2.8V/MCM-41: (a) hydrated at ambient conditions, (b) dehydrated at 723 K, (c) rehydrated at ambient conditions, and (d) hydrothermally treated.

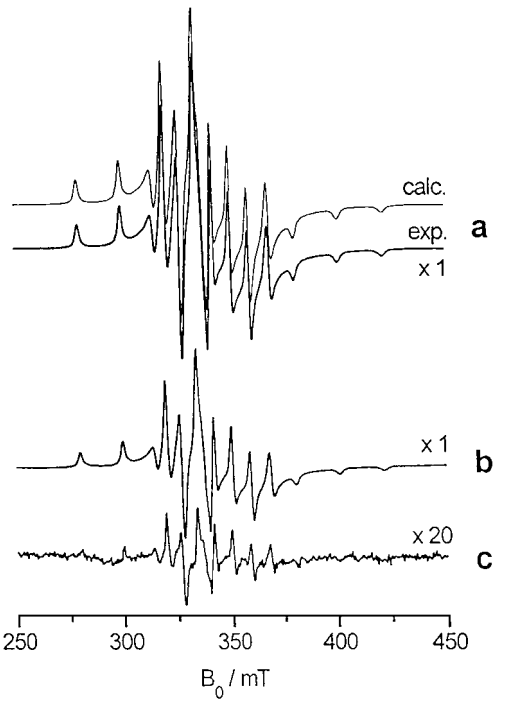

FIG. 6. ESR spectra at 77 K of V/MCM-41 samples freshly prepared: (a) 5.5V/MCM-41 experimental and calculated using parameters of Table 4, (b) 2.8V/MCM-41, and (c) 1.1V/MCM-41.

lowest vanadium content and seems to be present in comparable amounts in the higher loaded samples. A similar behaviour of isolated vanadium oxide species was already observed by Luan *et al.* (45) on V/MCM-41 samples prepared by means of *in situ* incorporation of the vanadium upon synthesis of those materials.

A NMR spectrum of a catalyst sample treated in a flow of 12 vol% water vapour in O_2 at 823 K is also shown in Fig. 5d. Part of the pseudo-tetrahedral coordinated V^V species seems to be increased. Considering ESR results (see below) this finding may be explained by an oxidation of V^{IV} to V^V species, which are still incorporated into the pore walls and, therefore, unable to coordinate water molecules.

ESR Results

In the ESR spectra of all freshly prepared V/MCM-41 samples the characteristic hyperfine splitting (hfs) multiplets of well-isolated vanadyl species in square pyramidal or distorted octahedral coordination are observed (Fig. 6) which frequently occur in vanadium-doped molecular sieves (49, 50). For vanadium loadings higher than 1.1 wt% the hyperfine signals are superimposed by a broad isotropic line which indicates the presence of interacting vanadyl species. Spectra simulation revealed that the latter compose the majority of the V^{IV} species observable in the spectra measured at 77 K (Table 4). At low vanadium loadings no isotropic singlet appears, pointing to higher dispersion of the V^{IV} sites. Moreover, it can be seen that the experimental spectra of freshly calcined samples 1.1V/MCM-41, 2.8V/MCM-41, and 5.5V/MCM-41 can be well fitted assuming only one single type of isolated vanadyl(IV) species. This holds also for sample 5.5V/MCM-41, having been used in a catalytic test. Obviously, the coordination symmetry of the V^{IV} sites is stable during time on stream.

The overall intensity of the ESR spectra (Fig. 6) and, thus, the total amount of the observed V^{IV} sites increases with

TABLE 4

g and hfs Tensor Parameters ($g_\parallel$, $g_\perp$) and Relative Intensities (I_{rel}) of Calculated ESR Subspectra

Sample	Species	$g_\parallel$	$g_\perp$	$A_\parallel$ (mT)	$A_\perp$ (mT)	$\Delta g_\parallel/\Delta g_\perp$[a]	I_{rel} (%)
5.5V/MCM-41	1	1.9368	1.9800	20.25	7.46	2.94	12.6
	2	1.9764		—		—	87.4
2.8V/MCM-41	1	1.9368	1.9800	20.25	7.46	2.94	16.8
	2	1.9764		—		—	83.2
2.8V/MCM-41	1	1.9321	1.9769	20.42	6.94	2.76	10.4
treated in	2	1.9232	1.9815	19.96	7.56	3.80	8.4
O_2–H_2O	3	1.9171	1.9898	18.20	6.79	6.81	2.3
	4	1.9957		—		—	79.0
1.1V/MCM-41	1	1.9368	1.9800	20.25	7.46	2.94	100.0

[a] $\Delta g_\parallel/\Delta g_\perp = (g_\parallel - g_e)/(g_\perp - g_e)$.

the vanadium loading. This trend is in line with the average vanadium valence state determined by potentiometric titration and TPR (see Table 3). However, the intensity of the spectra is relatively low in comparison to the content of V^{IV} species amounting up to 50% of the total vanadium content as determined by potentiometric titration and TPR. Therefore, it was supposed that tetravalent vanadium species such as tetrahedrally coordinated V^{IV} species (49) or V^{IV}–V^{IV} pairs (52, 53) exist in the samples which are not ESR active at $T \geq 77$ K due to short relaxation times. Therefore, ESR spectra were also measured below 77 K (Fig. 7). For this study a sample of 2.8V/MCM-41 was used which was hydrothermally pretreated in context with the investigation of the action mode of steam cofed in the catalytic testing. The asymmetric shape of the outermost lines of the A_{II} hfs signal indicates that this sample, in contrast to the freshly calcined one, contains more than one type of isolated V^{IV} site. This finding is confirmed by spectra simulation. At least three different subspectra for isolated species had to be superimposed to obtain a satisfactory fit of the experimental spectrum (Table 4). For two of these, the $\Delta g_{\|}/\Delta g_{\perp}$ values, being a measure for the tetragonal distortion of the vanadium coordination sphere, are markedly larger than in the fresh sample. This suggests that on treatment with water vapour the geometry of the vanadyl sites is further distorted, presumably by partial cleavage of V–O–Si bonds. In this way, species may be formed in which the V^{IV} is not only coordinated to bridging but also to terminal oxygen atoms, e.g., to OH groups in $V^{IV}O(OH)_x(H_2O)_2(OSi\equiv)_{2-x}$ surface species. Whereas the ESR intensity in the range of the hfs signal (250–450 mT) follows a Curie-like behaviour as expected for pure paramagnetic species, the additional broad signal around 175 mT rapidly disappears with increasing temperature and completely vanishes above 40 K (Fig. 7). Position and shape of this line are not compatible with tetrahedrally coordinated V^{IV} centres with a spin of $S = 0.5$ (51). However, the line may be due to pairs of V^{IV} centres with a total spin of $S = 1$ or V^{III}, having the same spin system (52–54). In any case, this low-field signal suggests the presence of reduced vanadium species which are not ESR active above 40 K but, nevertheless, contribute to the rather low average vanadium valence state determined by potentiometric titration and TPR (see Table 3).

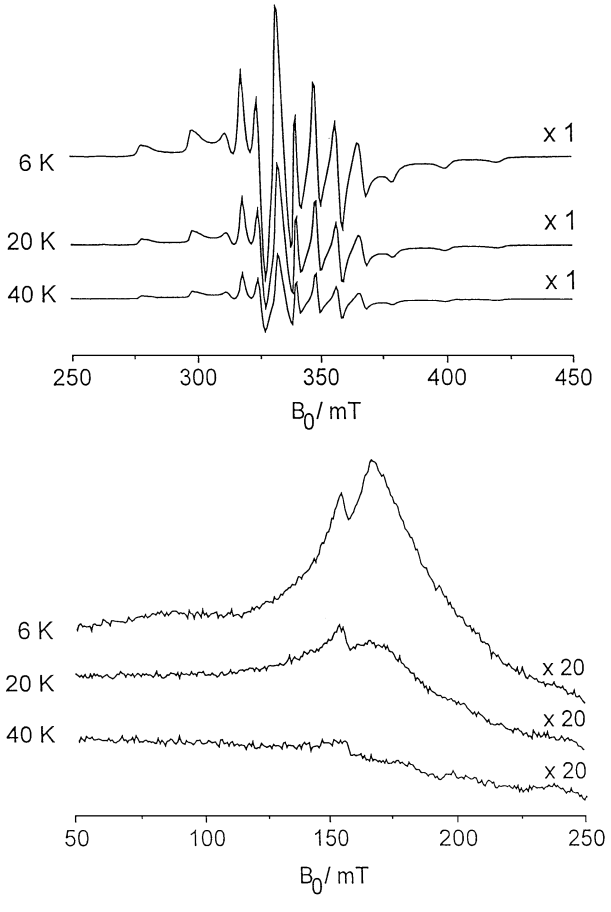

FIG. 7. ESR spectra below 77 K of sample 2.8V/MCM-41 after treatment in an argon flow containing 12 vol% water vapour for 0.5 h at 873 K.

UV-Vis Spectroscopic Results

The room temperature UV/VIS-DRS spectrum (Fig. 8 a) of sample 2.8V/MCM-41 (pretreatment: 0.5 h at 873 K in an argon flow containing 12 vol% water vapour for 0.5 h at 873 K) can be deconvoluted into 5 Gaussian lines which are assigned to monomeric (243 and 315 nm) and oligomeric tetrahedrally coordinated V^V species (360 nm) as well as to square pyramidal (412 nm) and distorted octahedral V^V species (458 nm) (34, 55). On heating the sample in flowing nitrogen to 823 K the bands at 412 and 458 nm disappear. This is caused by the release of water from the coordination sphere of V^V, leaving behind tetrahedrally coordinated V^V which additionally contributes to the bands at 235 and 294 nm (Fig. 8b). This process is reversible when the sample is exposed to ambient atmosphere.

Switching from N_2 flow to a mixture of 5% H_2–N_2 at 823 K leads to the partial reduction of V^V. This is indicated by the appearence of two bands for *d–d* transitions at 520 and 658 nm (Fig. 8c) the position of which is rather in agreement with V^{III}, than with V^{IV}. For example, in the $V(H_2O)^{3+}$ ion of vanadium alum the *d–d* transitions are located at 397 and 581 nm (56). In contrast, *d–d* transitions of tetravalent vanadium are red-shifted, e.g., 625 and 769 nm for VO^{2+} ions (57). Reoxidation in a flow of dry oxygen oxidizes the reduced species and leaves behind only tetrahedrally coordinated V^V composed by the charge-transfer (CT) bands in Fig. 8d.

Admixture of water vapour to the oxygen flow at 823 K does not create bands above 400 nm, characteristic of square pyramidal or octahedral V^VO_x species (Fig. 8e). Probably, the interaction of H_2O molecules with V^VO_x species at such high temperatures is too weak for a stable

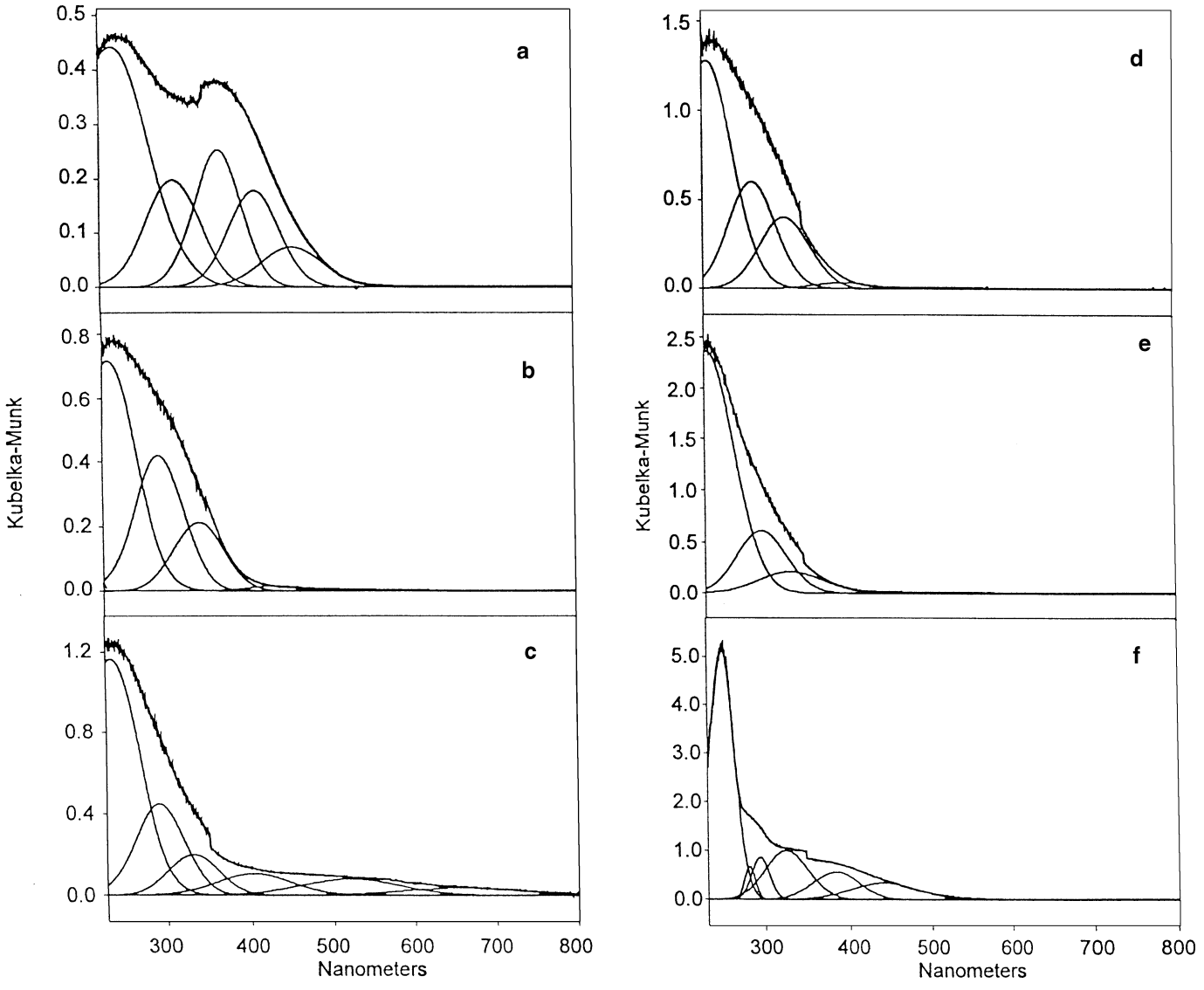

FIG. 8. Experimental (bold lines) and deconvoluted (weak lines) *in situ* UV/VIS-DRS spectra of a hydrothermally pretreated 2.8V/MCM-41 sample during the following successive treatment: (a) 293 K, N_2; (b) 823 K, N_2, 45 min; (c) 823 K, 5% H_2/N_2, 60 min; (d) 823 K, O_2, 60 min; (e) 823 K, O_2 flow containing 18 vol% H_2O 75 min; (f) 293 K, N_2.

extension of the coordination sphere. However, it can be seen that the band of tetrahedral V^VO_x species (232 nm) markedly increases during the oxidative treatment in the presence of water vapour. The effect is even more evident in a comparison of the room temperature spectra before and after the whole *in situ* UV/VIS-DRS experiment (Figs. 8a and 8f). This points to an oxidation of V^{IV} to V^V. It is interesting to note that the increase of V^V–CT bands is markedly less pronounced in a flow of dry oxygen. This suggests that in the presence of O_2 and H_2O preferably those $V^{IV}O_x$ species are oxidized which are not easily accessible on the surface because they are incorporated in the walls of V/MCM-41. Probably, water supports the penetration of oxygen into deeper layers of the MCM-41 structure by temporal cleavage of Si–O–Si bonds and, thus, enhances the mobility of the amorphous framework of the pore walls.

FTIR Spectroscopic Results

IR spectra of pyridine adsorbed on MCM-41 and on the 2.8V/MCM-41 catalysts are shown in Fig. 9. In the spectrum of the parent MCM-41 a band at 1445 cm^{-1} appears assigned to pyridine coordinatively bound to defect sites of a distorted silica network as weak acidic Lewis sites (58), or to hydrogen-bonded pyridine (59). The spectrum of the catalyst additionally shows a weak band at 1545 cm^{-1} which can be attributed to pyridinium cations formed on acid V–OH groups (Brønsted sites). The intensity of this band is

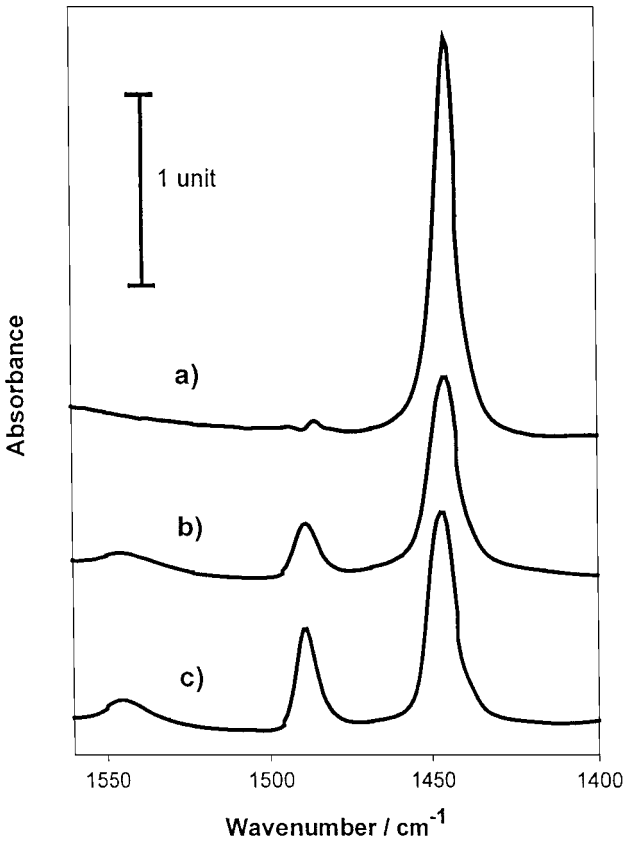

FIG. 9. FTIR spectra of pyridine adsorbed on the samples: (a) MCM-41, (b) 2.8V/MCM-41, and (c) 2.8V/MCM-41 hydrothermally treated.

slightly increased in the spectrum of the hydrothermally treated catalyst sample, pointing to formation of additional V–OH groups. The temperature-programmed pyridine desorption revealed a moderate acid strength of the Brønsted sites because pyridine was completely removed at 473 K already. Monomeric or mononuclear $V^{V}O(OH)(OSi\equiv)_2$ surface species, i.e., vanadium oxide species only twice anchored to the wall of the MCM-41, have been previously discussed by Grubert *et al.* (33), who studied the reduction mechanism of VO_x species on MCM-41. The presence of a single V–O–Si bridge and two V–OH groups was concluded by Shulman *et al.* from EXAFS results for "VO_4 clusters" on silica (60).

The OH vibration spectra of the catalyst before and after steaming are shown in Fig. 10. These spectra indicate that both samples contain similar kinds of silanol groups, however, in different proportions. The narrow vibration band at 3746 cm^{-1} belongs to isolated terminal silanol groups. The shoulder at 3710 cm^{-1} is attributed to hydrogen-bonded terminal hydroxyl groups ($SiOH\cdots{}^{-}OSi$) in the walls (59). The broad absorption band between 3700 and 3300 cm^{-1} (centered at ca. 3550 cm^{-1}) is due to OH-stretching vibrations of geminal and associated terminal silanol groups located on the pore walls of the support (35, 61, 62). The untreated sample contains a high portion of associated silanol groups as revealed by the high intensity of the broad absorption band at 3550 cm^{-1}. In contrast, the intensity of the 3746 cm^{-1} band of isolated terminal silanol groups is comparatively low. After treatment with steam at 873 K, the intensity of the band of associated silanol groups is distinctly decreased, whereas the intensity of the vibration band of isolated terminal silanols at 3746 cm^{-1} is markedly increased, although the sample was cooled to 373 K under water vapour before the IR spectrum was taken. These intensity changes reveal that the amount of isolated silanol groups is increased at the expense of associated silanol groups and conclusively points to a structural rearrangement of the support surface as recently claimed for water treatment under milder conditions (35). N_2 adsorption measurements confirmed that the mesoporous structure of the 2.8V/MCM-41 sample was not destroyed. The significant increase of the band at 3660 cm^{-1} pointed to formation of additional V–OH groups by hydrolysis of V–O–Si bridges. This was supported by the results of the pyridine adsorption, showing an increase of the band for pyridinium cations at 1545 cm^{-1}.

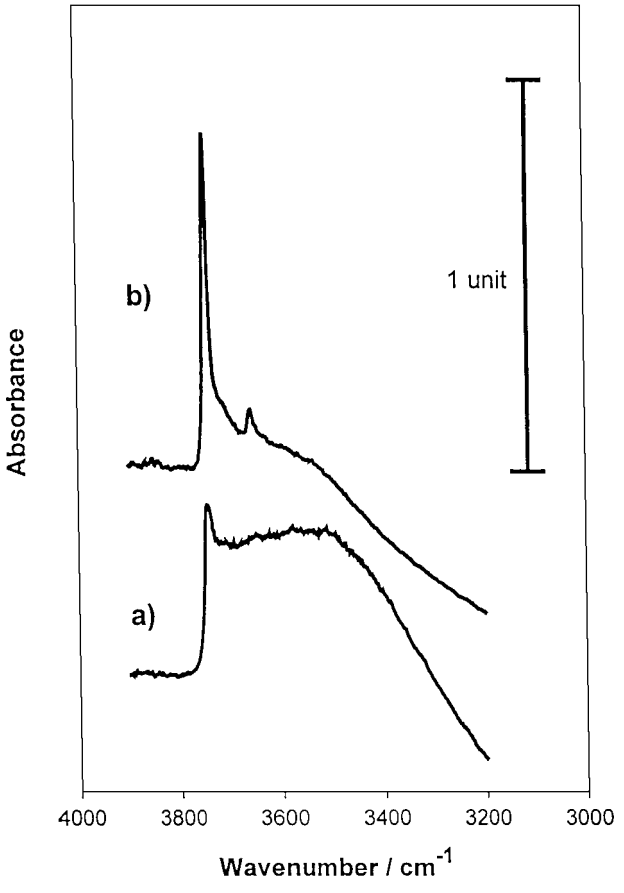

FIG. 10. FTIR spectra of the sample 2.8V/MCM-41 in the OH vibration region: (a) wafer evacuated at 473 K and (b) wafer *ex situ* hydrothermally pretreated and afterward evacuated in the IR cell at 373 K.

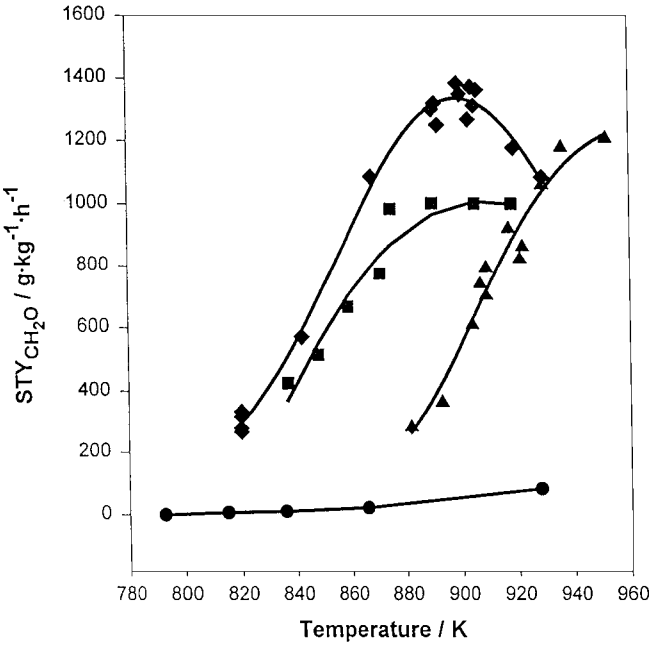

FIG. 11. Temperature dependence of the formaldehyde production on MCM-41 and VO_x/MCM-41 catalyst, containing different amounts of vanadium: (●) MCM-41, (▲) 1.1V/MCM-41, (◆) 2.8V/MCM-41, (■) 5.5V/MCM-41. CH_4 : air = 1.14; GHSV = 180,000 l · kg^{-1} · h^{-1}.

Catalytic Properties

Temperature dependence of the formaldehyde production on VO_x/MCM-41 samples with increasing vanadium loading was studied using a methane : air ratio and a GHSV typically applied for VO_x/SiO_2 catalysts by Herman *et al.* (3), who achieved the highest STY of formaldehyde (STY_{CH_2O}) up to now. Figure 11 shows the temperature dependence of the STY_{CH_2O} on catalyst samples with different vanadium content as well as on the parent MCM-41 using a GHSV = 180,000 l · kg^{-1} · h^{-1} and a feed composition of 53.2 vol% methane and 46.8 vol% air. The STY_{CH_2O} obtained with the samples 1.1V/MCM-41 and 2.8V/MCM-41 pass through maxima accompanied by a rise in carbon oxide formation, mainly carbon monoxide. The enhancement of the vanadium loading from 1.1 to 2.8 wt% results in a shift of the curve to lower temperatures at the same level of maximum STY_{CH_2O}. A doubling of the vanadium loading did not lead to increased formaldehyde production. Only the carbon oxide formation was drastically enhanced accompanied by considerable thermal fluctuation in the catalyst bed. Obviously, the consecutive oxidation of the desired product is favoured when the density of the VO_x sites in the tubular pores is too high. Further investigations were predominantly performed with VO_x/MCM-41 samples containing 2.8 wt% vanadium.

Table 5 presents results of the catalytic testing of the catalysts 2.8V/MCM-41* and 2.8V/MCM-41 in the temperature range of the maximum formaldehyde production. Comparable conversions, selectivities, and STY_{CH_2O} were obtained independently of the use of a V(IV) or a V(V) salt for impregnation of the MCM-41.

Arrhenius plots of the formaldehyde production on the catalysts 1.1V/MCM-41 and 2.8V/MCM-41 at low methane conversion are shown in Fig. 12. Apparent activation energies were determined from the fairly linear region of the plots obtained at two different GHSV. Approximately equal values were obtained for both catalysts.

In order to study the influence of the partial pressures of methane and oxygen, respectively, catalytic experiments at constant temperature and GHSV were performed. The latter was balanced by nitrogen added to the methane-air stream. Results of measurements with various methane and constant oxygen pressure (9.9 kPa) and with different oxygen pressure and constant methane pressure (53.7 kPa) are demonstrated in Fig. 13. The formaldehyde formation linearly increases with raising methane partial pressure, corresponding to a reaction order of $n = 0.83$ with respect to methane. On the other hand, the variation of the oxygen pressure did not significantly influence the formaldehyde production (reaction order of $n_{O_2} = -0.03$). Similar results of kinetic studies were previously reported by Sexton *et al.*

TABLE 5

Results of Catalytic Testing[a]

Catalyst	T (K)	STY_{CH_2O} (mol · kg^{-1} · h^{-1})	STY_{CH_3OH} (mol · kg^{-1} · h^{-1})	X_{CH_4} (mol%)	S_{CH_2O} (mol%)	S_{CH_3OH} (mol%)
2.8V/MCM-41*	868	33.5	0.8	3.0	28.4	0.7
	897	44.2	1.1	6.6	17.2	0.4
	924	44.6	1.2	9.3	12.3	0.3
2.8V/MCM-41	868	36.1	0.8	3.2	29.1	0.6
	899	46.1	1.4	5.4	22.0	0.2
	906	45.4	0.9	9.9	11.7	0.2
	929	36.1	0.7	11.0	8.4	0.2

[a] GHSV = 180,000 l · kg^{-1} · h^{-1}; CH_4 : air = 1.14.
*Precursor $VO(C_2O_4)$.

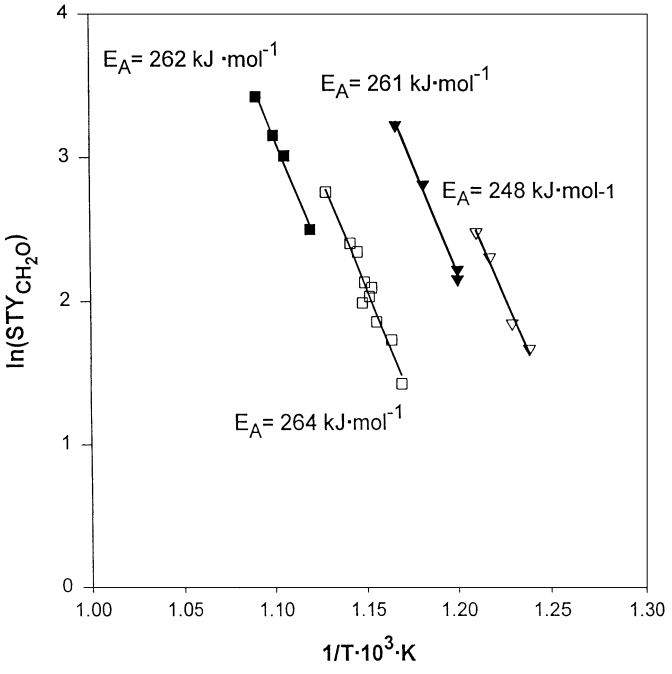

FIG. 12. Arrhenius plots of the formaldehyde production at different GHSV: CH_4 : air = 1.14, (■) 1.1V/MCM-41, (▼) 2.8V/MCM-41, (hollow symbols) GHSV = 90,000 $l \cdot kg^{-1} \cdot h^{-1}$, (filled symbols) GHSV = 180,000 $l \cdot kg^{-1} \cdot h^{-1}$.

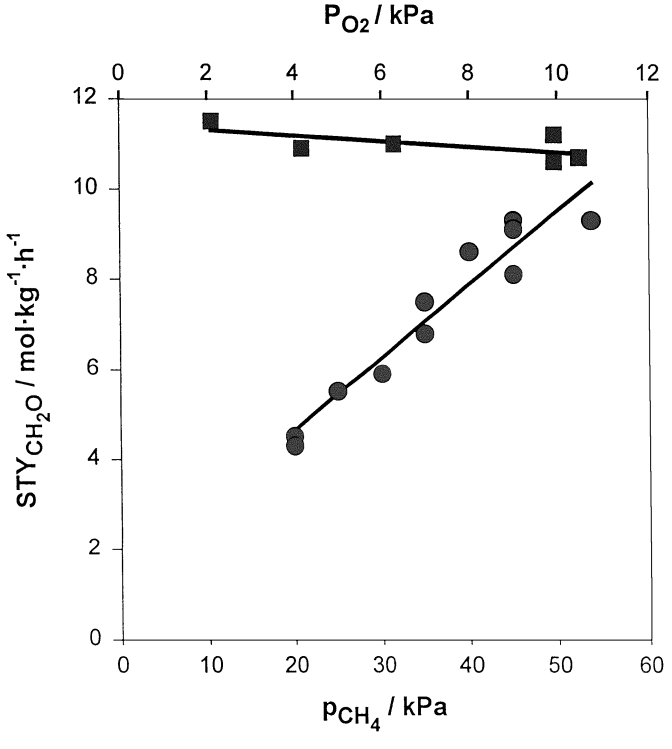

FIG. 13. Formaldehyde production dependent on the partial pressure of methane (●) and oxygen (■), respectively; GHSV = 180,000 $l \cdot kg^{-1} \cdot h^{-1}$; $T = 820$ K.

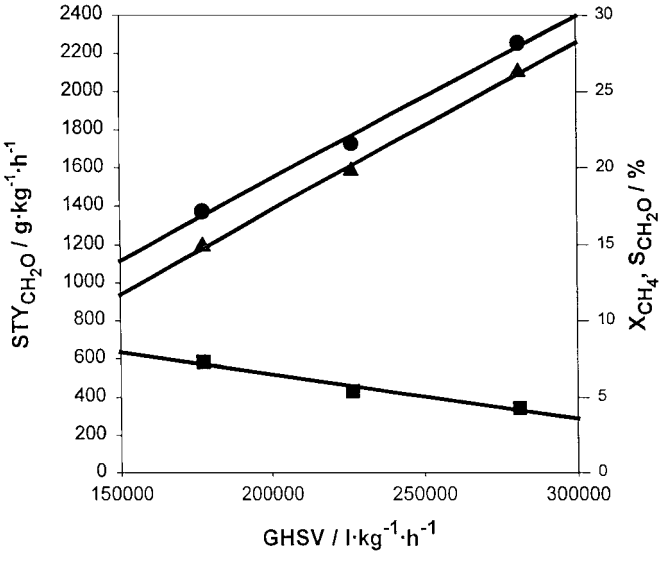

FIG. 14. Dependence of the space-time yield of formaldehyde (●), methane conversion (■), and formaldehyde selectivity (▲) on the gaseous hourly space velocity, sample 2.8V/MCM-41, $T = 900$ K; CH_4 : air = 1.14.

(27). A comparable activation energy for the formaldehyde production (242 kJ/mol) and reaction orders of $n_{CH_4} = 1.0$ and $n_{O_2} = 0$ have been obtained on a VO_x/Cab-O-Sil catalyst containing 1 wt% vanadium. Obviously, active VO_x sites of comparable intrinsic activity are present on the surface of silica and siliceous MCM-41.

Furthermore, the influence of the GHSV on the STY_{CH_2O} was studied at the temperature of the maximum formaldehyde production using the catalyst 2.8V/MCM-41 (Fig. 14). As expected, the methane conversion decreases with increasing modified residence time but only slightly. However, the STY_{CH_2O} rises due to an increasing formaldehyde selectivity, overcompensating the low conversion decrease.

The productivities of the VO_x/MCM catalysts were compared in Table 6 with the best result obtained in the last decade for conventional VO_x/SiO_2 catalysts (3). Significant higher values for the STY_{CH_2O} were achieved at comparable GHSV.

Cofeeding of Steam

Water vapour was added to the feed, whereby the educt flow was balanced with N_2; i.e., the GHSV and the methane : air ratio were held constant. First, the catalyst was tested using the dry educt flow, then in the presence of 18 vol% steam cofed, and finally without steam addition again. A period of 1 h each was applied every time to equilibrate the system. The results obtained in this way are demonstrated in Fig. 15. An essential rise of the formaldehyde production in addition to a significant increase of the methanol production could be observed during the cofeeding of steam.

TABLE 6

Space-Time Yields Achieved with the VO_x/MCM Catalyst Compared to the Best Result Reported in the Literature

Catalyst reactor type educt composition	GHSV ($l \cdot kg^{-1} \cdot h^{-1}$)	T (K)	STY_{CH_2O} ($g \cdot kg^{-1} \cdot h^{-1}$)	STY_{CH_3OH} ($g \cdot kg^{-1} \cdot h^{-1}$)	S_{CH_2O} (mol%)	S_{CH_3OH} (mol%)	X_{CH_4} (mol%)
2.8V/MCM-41 CPFR[a,b]	28,0000	895	2255	40	26.3	0.4	4.7
2.8V/MCM-41* CPFR[b]	28,0000	896	1900	100	22.6	0.5	4.6
2.8V/MCM-48 CPFR[b]	28,0000	898	1950	60	26.4	0.8	4.0
2% V_2O_5/SiO_2 CPFR[c] Ref. (3)	23,7000	898	1280	276	30.3	6.1	4.4

[a] CPFR, continuous plug flow reactor.
[b] CH_4 : air = 1.13.
[c] CH_4 : air : steam = 1.5 : 1 : 1.7.

However, the selectivity for formaldehyde is only slightly changed. The productivity for the two oxygenates before and after water vapour addition is comparable, pointing to any reversible change of the catalyst structure discussed below.

DISCUSSION

In this work the potential of novel vanadium oxide catalysts for the heterogeneous catalytic oxidation of methane to formaldehyde was investigated. Mesoporous M41S materials were used as supports which possess relatively stable surface areas and pores of relatively large diameter.

The structural characterization of the catalyst system VO_x/MCM-41 has shown that a high and thermally stable dispersion of vanadium oxide can be obtained on mesoporous supports. Furthermore, the density of the VO_x species (sites/m^2) is essentially lower at a given vanadium oxide loading in comparison to VO_x/SiO_2. Consequently, the facilities for a total oxidation of surface intermediates of the formaldehyde formation on isolated sites in the neighbourhood are restricted.

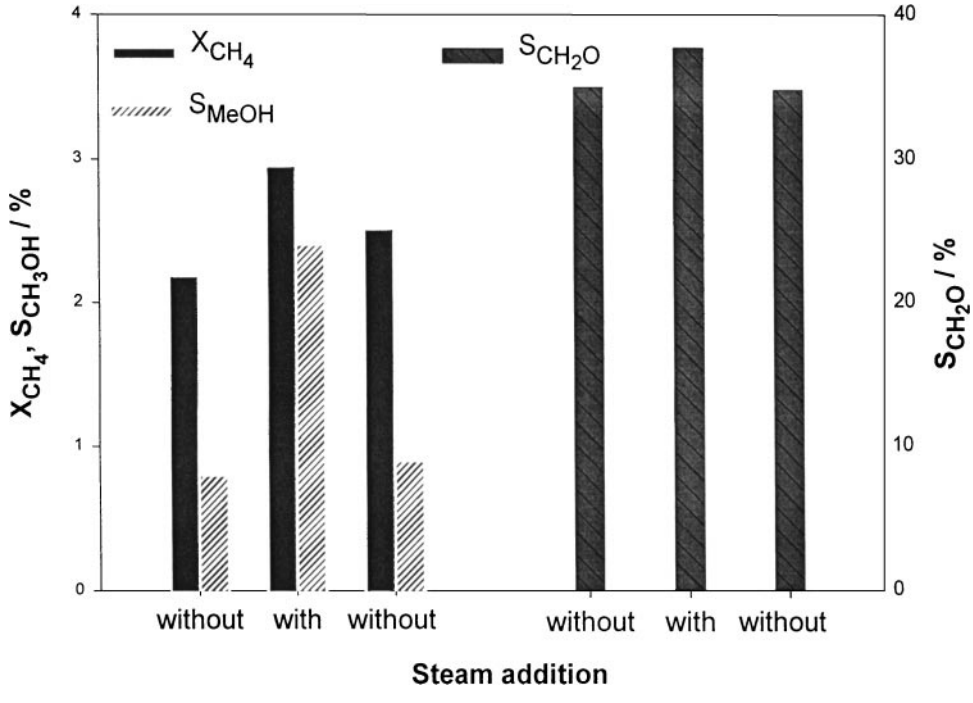

FIG. 15. Influence of steam cofed on methane conversion and selectivity of formaldehyde and methanol production, respectively; sample 2.8V/MCM-41, GHSV = 300,000 $l \cdot kg^{-1} \cdot h^{-1}$; CH_4 : air : N_2 or H_2O = 1.16 : 1 : 0.39; T = 895 K.

Characterization of the valence state of the vanadium oxide species by means of TPR and potentiometric titration revealed that such catalysts contain a significant amount of vanadium in a valence state lower than 5. This finding was rather surprising because the samples were not prepared by *in situ* incorporation of vanadium as reported in Ref. (45) but by deposition of vanadium precursor species on the support via impregnation with aqueous $VO(C_2O_4)$ or NH_4VO_3 solution followed by a calcination in air for a long time (16 h). Probably, vanadyl(IV) species impregnated or formed from the vanadate species via reduction by ammonia are incorporated into the amorphous walls of the mesoporous silica material and, thus, stabilized against oxidation.

Investigations by means of ^{51}V NMR, UV-Vis, and ESR spectroscopy, respectively, have confirmed that portions of V^{IV} as well as V^{V} species are located inside the walls. V^{IV} species only observed by ESR when the spectrum is recorded below 77 K point to paired V^{IV} species incorporated into the walls. *In situ* UV-Vis spectrometric studies have shown that such V^{IV} species can be easier oxidized by oxygen under hydrothermal conditions than in dry atmosphere. The formation of additional tetrahedrally coordinated V^{V} species was confirmed by corresponding ^{51}V NMR results. Obviously, the penetration of oxygen to the V^{IV} species inside the pore walls is supported by water vapour strongly interacting with the MCM-41 surface. Moreover, ^{51}V NMR measurements revealed the presence of pseudo-tetrahedrally coordinated $V^{V}O_x$ species in samples stored under wet air for a long time. This means that also a part of V^{V} species either is inaccessible to water vapour or does not additionally coordinate water. Therefore, it can be concluded that these species should be also incorporated into the pore walls of the support and, consequently, should also not be involved in the catalytic reaction as the incorporated V^{IV} species.

The nature and properties of the $V^{V}O_x$ species anchored to the pore walls of the support are comparable to those of conventional VO_x/SiO_2 catalysts in particular with respect to their structure and redox behaviour. Moreover, a similar apparent activation energy and comparable reaction orders of the formaldehyde production with respect to methane and oxygen, respectively, point to similar active sites.

A partial diffusion constraint of the formaldehyde production in the tubes of the M41S materials cannot be excluded. So an influence of the particle size of mesoporous materials on STY_{CH_2O} and Y_{CH_2O} was recently observed on mesoporous MoO_x/SBA-1 catalysts by Tatsumi and Hamakawa (63). However, we think that the diffusion constraint in the small pores of conventional VO_x/SiO_2 catalysts is not lower but rather higher than the one in the uniform relatively wide pore system of the M41S materials.

As described for VO_x/SiO_2 catalysts in Ref. (3) a promoting action of cofed steam was also observed for VO_x/MCM-41 catalysts. The enhanced formation of methanol in the catalytic reaction can be attributed to an increased hydrolysis of surface methoxy species formed as intermediate as already proposed by Herman *et al.* (3). However, what could be the reason for the enhanced methane conversion accompanied by a small increase of the formaldehyde selectivity? In principle, a generation of additional active sites and/or a structural transformation of the existing active sites can be supposed, which result in an increased activity.

TPR has revealed an increase of the high temperature flank at the expense of the low temperature peak. Probably, a surface migration of monomeric VO_x species occurs, resulting in a portion of oligomeric vanadium oxide species as observed by UV-Vis spectroscopy. However, the intrinsic activity of such species relative to that of monomeric vanadium oxide species is not known.

An increase of the amount of active sites could result from the oxidation of $V^{IV}O_x$ species located inside the walls to $V^{V}O_x$ species in connection with their accessibility under enhanced water vapour pressure as indicated by TPR as well as spectroscopic results.

Furthermore, a formation of V–OH groups has been observed by means of FTIR/pyridine adsorption. Moreover, ESR results have also pointed to a formation of V^{IV} surface species carrying OH groups. It is conceivable that oxidic vanadium species carrying a V–OH group are the genuine active sites for the methane activation. On the one hand, a V–OH group would be easier to reduce than a V–O–Si bridge (33) and the reduced specimens could be active sites for a concerted action with gas-phase oxygen as proposed in Refs. (24, 25). On the other hand, hydroxylated vanadium oxide species could also be the sites where "short-lived adsorbed oxygen species" can be coordinated and activate the methane molecule as supposed in Ref. (26). Because of a reversible promoting influence of water vapour we prefere a reversible cleavage and linking of V–O–Si bridges for an explanation of the observed significant acitvity changes.

On the basis of our results and considering the mechanisms mentioned above we propose in Fig. 16 a scheme of the formation of the active sites and their interaction with methane and oxygen: The hydrated form of the prepared catalysts contains square-pyramidal as well as pseudo-octahedral coordinated isolated $V^{V}O_x$ species (Ia, Ib) and a portion of bridged or low-oligomeric $(V^{V}O_x)_n$ species (Ic). Heating up in dry atmosphere results in a transformation to pseudo-tetrahedral coordinated $V^{V}O_x$ species (II). Under catalytic conditions, i.e., in the presence of water vapour formed or cofed, acidic $V^{V}O(OH)_x(OSi\equiv)_{3-x}$ species are formed (III) which can be reduced to $V^{IV}O(OH)_x(OSi_x\equiv)_{2-x}$ species (IV). Considering the proposed methane activation by interaction with oxygen activated on reduced sites (24, 25) or by interaction of methane with short lived oxygen species on VO_x species (26), we suggest two possibilities for this first step in the methane

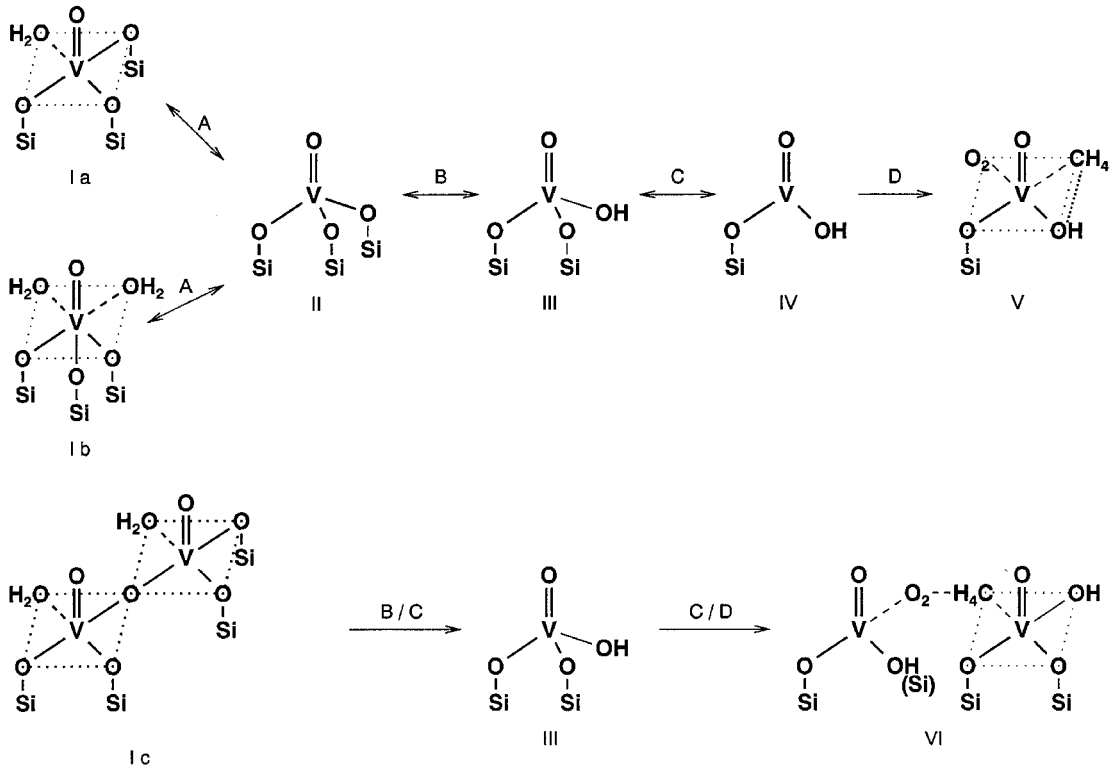

FIG. 16. Scheme of the formation of the active sites and their interaction with O_2 and CH_4: (Ia,b) coordinatively saturated V^VO_x species in the stored (hydrated) catalyst, (Ic) bridged (low-oligomeric) V^VO_x species in the catalyst, (II) isolated V^VO_x species in the dehydrated catalyst, (III) acidic V^VO^x species, (IV) acidic $V^{IV}O^x$ species ("reduced sites"), (V) adsorption complex of O_2 and CH_4 on one active species, (VI) adsorption complex on neighbouring "reduced site" and acid site, (A) reversible dehydration/hydration, (B) partial hydrolysis by water formed or cofed, (C) reduction to $V^{IV}O_x$ species under catalytic conditions, (D) coordination and activation of O_2 on a V^{IV} site and of CH_4 on an acidic V^{IV} or V^V site.

conversion to formaldehyde. On the one hand, CH_4 and O_2 could be coordinated on the same acidic reduced site (V). Methane is activated in the formed species by interaction with coordinated O_2 as well as with the acidic OH group. On the other hand, O_2 and CH_4 could be coordinated on neighbouring sites (VI), i.e., O_2 on a reduced site and CH_4 on an acidic V^V or V^{IV} species. Also in this case a "concerted mechanism" on reduced and acid sites is conceivable as suggested in Ref. (25).

In summary, the application of the high surface area mesoporous siliceous materials MCM-41 and MCM-48 as supports instead of conventional silica materials leads to catalysts with similar or equal active sites as on VO_x/SiO_2 catalysts. However, a higher concentration of monomeric or low-oligomeric vanadium oxide species can be achieved at low density of these sites. Employing these catalysts the STY_{CH_2O} could be essentially improved in the partial oxidation of methane (64).

Despite this progress, an industrial application of the partial methane oxidation to formaldehyde in an individual process would still be insufficient because the methane conversion and the formaldehyde yield are low at single pass of the educt stream. Higher yields can be obtained in a process with a reactor, operating in "continuous flow recycle mode" with formaldehyde separation as previously reported by Zuev *et al.* (65) and recently again proposed by Parmaliana *et al.* (22). However, only low STY_{CH_2O} was obtained in this way because of the low activity of the catalyst used in order to achieve a high selectivity.

On the other hand, it is conceivable that a process of methane partial oxidation with single pass of the educt stream could be combined with a large-scale methane steam reforming process in order to improve the exploitation of the feedstock. In this case, the exit gases of the methane partial oxidation could be added to the educt stream of the converter for synthesis gas production. Particularly promising for the feasibility of a formaldehyde process appears the use of highly active catalysts in wall reactors with water films on condensor areas for protection of the formaldehyde against consecutive oxidation (20, 21). Only relatively low catalyst amounts can be employed as layers in such kind reactors and therefore, use of catalysts optimized concerning their productivity may be favourable. Steam cofeeding for generation of the water film would not restrict the activity of V/MCM catalysts but the STY_{CH_2O} would even be increased.

CONCLUSIONS

Mesoporous siliceous materials of the family M41S were succesfully applied as supports to develop improved vanadium oxide-based catalysts for the partial oxidation of methane to formaldehyde by air. The high and thermally stable surface areas of siliceous MCM-41 and MCM-48 are favourable for achieving a high concentration of isolated vanadium oxide species generally considered as active sites of the partial methane oxidation.

The characterization of the vanadium oxide species using several established methods led to two surprising findings:

(i) Oxide species of the four valent vanadium are present beside those of the five valent vanadium, despite calcination of the catalyst precursor in air.

(ii) Portions of the $V^{IV}O_x$ species as well as of the $V^{V}O_x$ species are located inside the pore walls although the vanadium oxide precursor was deposited on the support by impregnation.

The structure of the species anchored by V–O–Si bridges to the pore walls is comparable to that for VO_x/SiO_2 catalysts reported in the literature. However, it was proved that these species partially carry V–OH groups. The concentration of the latter rises by interaction of the catalyst surface with cofed steam, enhancing the STY_{CH_2O}. So, it was suggested that $V^{V}O(OH)_x(OSi{\equiv})_{3-x}$ or "corresponding reduced sites" $V^{IV}O(OH)_x(OSi{\equiv})_{2-x}$ are the real active sites in these catalysts under reaction conditions. Employing VO_x/MCM catalysts the STY_{CH_2O} could be significantly improved to about 2.2 $kg \cdot kg_{cat}^{-1} \cdot h^{-1}$.

ACKNOWLEDGMENTS

The assistance of Mrs. S. Evert in the catalyst characterization as well as Mrs. U. Wolf in the FTIR spectroscopic investigations is gratefully acknowleged. The authors thank the Federal Ministry of Education and Research, Germany, as well as the Science Department of the Senate of Berlin for financial support (Project No. 03 C3012 0).

REFERENCES

1. Pitchai, R., and Klier, K., *Catal. Rev. Sci. Eng.* **28**, 13 (1986).
2. Brown, M. J., and Parkyns, N. D., *Catal. Today* **8**, 305 (1991).
3. Herman, G., Sun, Q., Shi, C., Klier, K., Wang, C.-B., Hu, H., Wachs, I. E., and Bhasin, M., *Catal. Today* **37**, 1 (1997).
4. Parmaliana, A., Frusteri, F., Mezzapica, A., Miceli, D., Scurrell, M. S., and Giordano, N., *J. Catal.* **143**, 262 (1993).
5. Miceli, D., Arena, F., Parmaliana, A., Scurrell, M. S., and Sokolovskii, V., *Catal. Lett.* **8**, 283 (1993).
6. Parmaliana, A., and Arena, F., *J. Catal.* **167**, 57 (1997).
7. Cardoso, J. H., Bañares, M. A., Correa Bueno, J. M., and Fierro, J. L. G., *Collect. Czech. Chem. Commun.* **63**, 1743 (1998).
8. Koranne, M. M., Goodwin, J. G., Jr., and Marcelin, G., *J. Catal.* **148**, 369, 388 (1994).
9. Sexton, A. W., Coda, E. M. G., and Hodnett, B. K., *Catal. Today* **46**, 127 (1998).
10. de Lucas, A., Valverde, J. L., Cañizares, P., and Rodriguez, L., *Appl. Catal. A* **172**, 165 (1998).
11. Kudo, H., and Ono, T., *Appl. Surf. Sci.* **121/122**, 413 (1997).
12. Otsuka, K., and Hatano, M., *J. Catal.* **108**, 252 (1987).
13. Solymosy, F., Tombacz, I., and Kutzan, G., *J. Chem. Soc. Chem. Commun.* 1455 (1985).
14. Baldwin, T. R., Burch, R., Squire, G. D., and Tsang, S. C., *Appl. Catal.* **71**, 137 (1991).
15. Spencer, N. D., *J. Catal.* **109**, 187 (1988).
16. Bañares, M. A., and Fierro, J. L. G., "ACS Symposium Series" (S. T. Oyama, and J. W. Hightower, Eds.), Vol. 523, p. 354. Am. Chem. Soc., Washington, DC, 1993.
17. Spencer, N. D., and Pereira, C. J., *J. Catal.* **116**, 399 (1989).
18. Alptekin, G. O., Herring, A. M., Williamson, D. L., Ohno, T. R., and McCormick, R. L., *J. Catal.* **181**, 104 (1999).
19. Batiot, C., and Hodnett, B. K., *Appl. Catal. A* **137**, 179 (1996).
20. Didenko, L. P., Linde, V. R., and Savchenko, V. I., *Catal. Today* **42**, 367 (1998).
21. Yu, L., Yuan, S., Wu, Z., Wan, J., Gong, M., Pan, G., and Chen, Y., *Appl. Catal. A* **171**, L171 (1998).
22. Parmaliana, A., Arena, F., Frusteri, F., and Mezzapica, A., *Stud. Surf. Sci. Catal.* **119**, 551 (1998).
23. Shi, C., Sun, Q., Hu, H., Herman, R. G., Klier, K., and Wachs, I. E., *Chem. Commun.*, 663 (1996).
24. Parmaliana, A., Sokolovskii, V., Miceli, D., Arena, F., and Goirdano, N., *J. Catal.* **148**, 514 (1994).
25. Parmaliana, A., Arena, F., Frusteri, F., Matra, G., Coluccia, S., and Sokolovskii, V., *Stud. Surf. Sci. Catal.* **110**, 347 (1997).
26. Kartheuser, B., Hodnett, B. K., Zanthoff, H., and Baerns, M., *Catal. Lett.* **21**, 209 (1993).
27. Sexton, A. W., and Hodnett, B. K., *Stud. Surf. Sci. Catal.* **110**, 1129 (1997).
28. Koranne, M. M., Goodwin, Jr., and Marcelin, G., Proceeding, Symposium Natural Gas Upgrading II ACS, San Francisco Meeting, April 5-10, 1992, p. 41.
29. Amiridis, M. D., Rekoske, J. E., Dumesic, J. A., Rudd, D. F., Spencer, N. D., and Pereira, C. J., *AIChE J.* **37**, 87 (1991).
30. Arena, F., Frusteri, F., Parmaliana, A., and Giordano, N., *Appl. Catal. A* **125**, 39 (1995).
31. Aoki, K., Ohmae, M., Nanba, T., Takeishi, K., Azuma, N., Ueno, A., Ohfune, H., Hayashi, H., and Udagawa, Y., *Catal. Today* **45**, 29 (1998).
32. Kresge, C. T., Leonowicz, M. E., Roth, W. J., Vartuli, J. C., and Beck, J. S., *Nature* **359**, 710 (1992); USP 5,098,684 and USP 5,102,643.
33. Grubert, G., Rathouský, J., Schulz-Ekloff, G., Wark, M., and Zukal, A., *Microporous Mesoporous Mater.* **22**, 225 (1998).
34. Morey, M., Davidson, A., Eckert, H., and Stucky, G., *Chem. Mater.* **8**, 486 (1996).
35. Landmesser, H., Kosslick, H., Storek, W., and Fricke, R., *Solid State Ionics* **101/103**, 271 (1997).
36. Kosslick, H., Lischke, G., Landmesser, H., Parlitz, B., Storek, W., and Fricke, R., *J. Catal.* **176**, 102 (1998).
37. Barett, E. P., Joyner, L. G., and Halenda, P. O., *J. Am. Chem. Soc.* **73**, 373 (1951).
38. Niwa, M., and Murakami, Y., *J. Catal.* **76**, 9 (1982).
39. Das, N., Eckert, H., Hu, H., Wachs, I. E., Walzer, J. F., and Feher, F. F., *J. Phys. Chem.* **97**, 8240 (1993).
40. Lozos, G. P., Hofman, B. M., and Franz, C. G., Quantum Chemistry Programs Exchange No. 265, 1973.
41. Kortüm, G., "Reflexionsspektroskopie." Springer-Verlag, Berlin, 1969.
42. Walker, J. F., "Formaldehyde," ACS Monograph Series. Reinhold, New York, 1953.
43. Arena, F., Giordano, N., and Parmaliana, A., *J. Catal.* **167**, 66 (1997).

44. Nag, K. N., and Massoth, F. E., *J. Catal.* **124**, 127 (1990).
45. Luan, Z., XU, J., He, H., Klinowski, J., and Kevan, L., *J. Phys. Chem.* **100**, 19595 (1996).
46. Lapina, O. B., Mastikhin, V. M., Nosov, A. V., Beutel, T., and Knözinger, H., *Catal. Lett.* **13**, 203 (1992).
47. Centi, G., Fazzini, F., Canesson, L., and Tuel, A., *Stud. Surf. Sci. Catal.* **110**, 893 (1997).
48. Eckert, H., and Wachs, I. E., *J. Phys. Chem.* **93**, 6796 (1989).
49. Wark, M., Brückner, A., Liese, T., and Grünert, W., *J. Catal.* **175**, 48 (1998).
50. Lohse, U., Brückner, A., Kintscher, K., Parlitz, B., and Schreier, E., *J. Chem. Soc. Faraday Trans.* **91**, 1173 (1995).
51. Hari Prasad Rao, P. R., Ramaswamy, A. V., and Ratnasamy, P., *J. Catal.* **137**, 225 (1992).
52. Brückner, A., and Zanthoff, H. W., *Colloids Surf. A* **158**, 107 (1999).
53. Abi-Aad, E., Bennani, A., Bonnelle, J. P., and Aboukais, A., *J. Chem. Soc. Faraday Trans.* **91**, 99 (1995).
54. Joyce, R. R., and Richards, P. L., *Phys. Rev.* **179**, 375 (1969).
55. Schraml-Marth, M., Wokaun, A., Pohl, M., and Krauss, H.-L., *J. Chem. Soc. Faraday Trans.* **87**, 2635 (1991).
56. Ballhausen, C. J., "Introduction to Ligand field Theory." McGraw-Hill, New York, 1962.
57. Centi, G., Perathoner, S., Trifiró, F., Abouakais, A., Aissi, C. F., and Guelton, M., *J. Phys. Chem.* **96**, 2617 (1992).
58. Kosslick, H., Lischke, G., Walther, G., Storek, W., Martin, A., and Fricke, R., *Microporous Mater.* **9**, 13 (1997).
59. Parry, E. P., *J. Catal.* **2**, 371 (1963).
60. Shulman, R. G., Yafet, Y., Eisenberger, P., and Blumberg, W. E., *Proc. Natl. Acad. Sci. USA* **73**, 1384 (1986); *in* "Catalyst Characterization" (B. Imelik and J. C. Vedrine, Eds.). Plenum, New York, 1992.
61. Eckert, H., Yesinowski, J. P., Silver, L. A., and Stolper, E. M., *J. Phys. Chem.* **92**, 2055 (1988).
62. Boehm, H. P., *Adv. Catal.* **16**, 226 (1966).
63. Tatsumi, T., and Hamakawa, N., Book of Abstracts EUROPACAT-4, Rimini, September 5–10, 1999, p. 557.
64. Berndt, H., Lücke, B., Evert, S., Martin, A., Schreier, E., Kosslick, H., and Wolf, G.-U., German patent application 199 10 145.0, 26. February, 1999.
65. Zuev, I. A., Vilenskii, A. R., and Mukhlenov, I. P., *J. Appl. Chem. (USSR) (Engl. Trans.)* **61**, 2389 (1988).